SCANNING VOL. 31, 1–8 (2010)

Unusual Secondary Electron Emission Behavior in Carbon Nanotube Forests

Md. K. Alam, P. Yaghoobi, and A. Nojeh

Department of Electrical and Computer Engineering, The University of British Columbia, Vancouver, British Columbia, Canada

Summary: Electron yield was measured from patterned carbon nanotube forests for a wide range of primary beam energies (400–20,000 eV). It was observed that secondary and backscattered electron emission behaviors in these forests are quite different than in bulk materials. This seems to be primarily because of the increased range of electrons due to the porous nature of the forests and dependent on their structural parameters, namely nanotube length, diameter and inter-nanotube spacing. In addition to providing insight into the electron microscopy of nanotubes, these results have interesting implications on designing novel secondary electron emitters based on the structural degrees of freedom of nanomaterials. SCANNING 31: 1–8, 2010. © 2010 Wiley Periodicals, Inc.

Key words: carbon nanotubes, scanning electron microscopy, electron beam-specimen interaction, secondary electron emission, nanostructures

Introduction

The measurement and study of secondary electron (SE) emission from solids have long been of interest for various reasons such as understanding and modeling different aspects of electron beam–solid interaction (Baroody 1950; Dekker 1960; Joy 1995a; McKay 1948; Reimer 1998; Schou 1988; Walker *et al.* 2008), as well as building new devices and equipment like electron multipliers, micro-channel plates and electron microscopes (Pendyala *et al.* 1974; Shapira *et al.* 2000). Carbon nanotubes (CNTs) are considered promising candidates for electron multipliers because of their excellent electron emission properties. They have been shown to enable robust, stable, low-voltage and high-brightness electron emitters (De Jonge and Bonard 2004; De Jonge *et al.* 2005; Hu *et al.* 2001; Yaghoobi and Nojeh 2007) and high electron gain (Kim *et al.* 2002; Nojeh *et al.* 2004; Yi *et al.* 2001). SE emission also plays a very important role in the imaging of CNTs (Brintlinger *et al.* 2002; Finnie *et al.* 2008; Homma *et al.* 2004; Wong *et al.* 2006), yet only a few reports exist in the literature on SE emission from CNTs. Electron yield from multi-walled carbon nanotube (MWNT) carpets (very wide forests with macroscopic dimensions) coated with different materials such as MgO, CsI and ZnO has mainly been reported so far (Huang *et al.* 2006; Kim *et al.* 2002; Lee *et al.* 2009; Yi *et al.* 2001). These studies reported SE emission yield from various samples under different conditions. For example, maximum electron yield from MgO-coated MWNTs was reported to be in the range of 21–22,000 from different MgO/MWNT samples (Kim *et al.* 2002; Lee *et al.* 2009; Yi *et al.* 2001). However, there is still much to be learnt about the SE emission behavior of bare CNTs. In this article, an experimental study of secondary and backscattered electron (BSE) emission from patterned CNT forests is presented for a wide range of primary beam energies. Experimental results are then explained using Monte–Carlo simulations and structural parameters of nanotube forests (diameter, length and inter-nanotube spacing).

Fabrication and Experiments

The CNT forests were fabricated using the following process: photoresist was coated on a highly doped p-type silicon substrate and circular patterns

Contract grant sponsors: Natural Sciences and Engineering Research Council (NSERC); Canada Foundation for Innovation (CFI); British Columbia Knowledge Development Fund (BCKDF); University of British Columbia Graduate Fellowship.

Address for reprints: A. Nojeh, Department of Electrical and Computer Engineering, The University of British Columbia, Kaiser 4041, 2332 Main Mall, Vancouver, BC, Canada V6T 1Z4
E-mail: anojeh@ece.ubc.ca

Received 7 December 2009; Accepted 12 January 2010

DOI 10.1002/sca.20169
Published online in Wiley InterScience (www.interscience.wiley.com)

with diameters varying from 50 to 500 μm were defined using photolithography. About 10 nm of aluminum and 2 nm of iron were then deposited using electron-beam evaporation. Circularly patterned catalyst islands of aluminum/iron were thus obtained after lifting-off the photoresist. Nanotube growth was done using chemical vapor deposition. A typical growth entailed heating the sample up to 750°C while flowing argon at 1,000 sccm until the temperature was stabilized. At 750°C, the sample was annealed for 3 min while reducing the flow rate of argon to 200 sccm and adding hydrogen at 500 sccm. Ethylene (at a rate of 20 sccm) was then introduced in the reaction chamber and the flow of argon and hydrogen were reduced to 120 sccm and 80 sccm, respectively for 30 min for CNT growth. This recipe grew forests as tall as 1 mm long consisting of MWNTs as confirmed by electron microscopy (Fig. 1).

The forests were then placed inside a Philips 525 M scanning electron microscope (SEM) chamber for the measurement of the secondary and BSE yield. The schematic of the experimental apparatus is shown in Figure 2. We followed a procedure similar to that used by others for the measurement of total electron yield (TEY) from various materials (Kim *et al.* 2002; Lee *et al.* 2009; Yi *et al.* 2001), as well as for SE and BSE coefficients (Huang *et al.* 2006; Sim and White 2005).

The primary beam current (I_P) was measured using a faraday cup and the specimen current (I_T) was measured with a high precision programmable Keithley 6517A electrometer (interfaced with a PC) at various primary beam energies (0.4–20 keV) for different bias values (+50 V, 0 V, −50 V, −100 V, −150 V, −200 V) applied by the electrometer's internal voltage source. The SEM detector was turned off throughout the experiments (except for initially bringing a forest under the beam and focusing on it). In all experiments, the primary beam was scanned over an area of $\sim 20 \times 15\ \mu m^2$ at the speed of 31.25 ms per frame (62.5 lines per frame and 0.5 ms per line) and positioned at the center of the top surface of the nanotube forest. Therefore, given that the smallest-diameter forest used in the experiments had a diameter of 50 μm (see the *Results* and *Discussion* section), the beam was always far away from the vertical sidewalls of the forest for all the specimens. The movement between the Faraday cup and the specimen was controlled by the automatic stage control system of the SEM. Each experiment was performed on a single forest, which was kept the same for the entire energy range for consistency.

At each value of specimen bias, the TEY, δ_T, (note that historically, in the literature the TEY is sometimes referred to as SE yield (Kim *et al.* 2002;

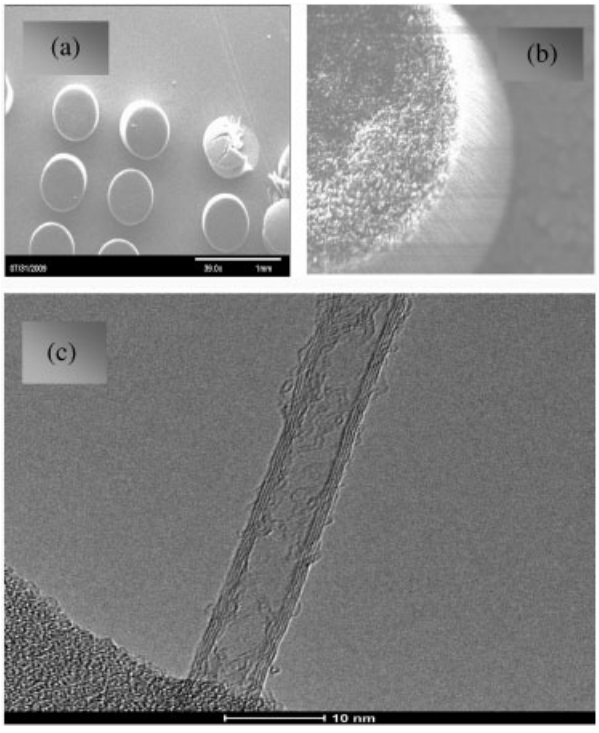

Fig 1. (**a** and **b**) Scanning electron micrographs of patterned nanotube forests. In (a) forests with a diameter of 500 μm and lengths of approximately 1 mm are shown. (b) shows a zoomed-in view of a 50 μm-diameter forest (field of view = 51.3 um). (**c**) Transmission electron micrograph of one individual nanotube extracted from the forest, revealing more detail about the nature of the grown nanotubes (muti-walled with diameters of the order of 10 nm).

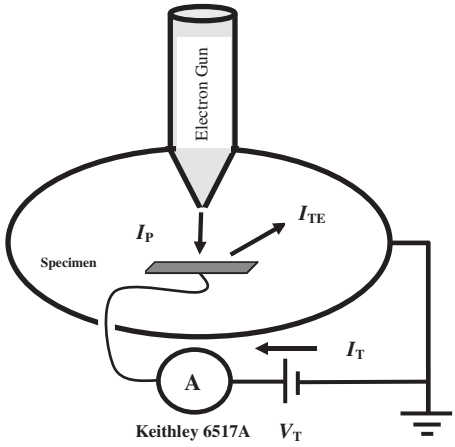

I_P = Primary beam current
I_{TE} = Total emitted electron current
I_T = Specimen current
V_T = Applied voltage to the specimen

Fig 2. Schematic of the experimental setup in the SEM (arrows show the assumed direction of current for which formulas are given in the calculations). The specimen (forest) is connected to the Keithley 6517A electrometer (internal voltage source and current meter are in series) using vacuum feed-throughs. The body of the SEM column and the chamber wall are grounded.

Lee *et al.* 2009; Yi *et al.* 2001). Here, to avoid confusion with SE coefficient, we chose the term TEY) was calculated using Equation (1).

$$\delta_T = \frac{I_{TE}}{I_P} = 1 + \frac{I_T}{I_P} \quad (1)$$

I_T and I_P were defined above and I_{TE} is the total emitted electron current. This is deduced from the fact that $I_{TE} = I_P + I_T$. The BSE coefficient, that is the ratio of the number of electrons exiting the specimen having kinetic energy greater than 50 eV to the number of primary electrons hitting the specimen, was calculated by measuring the primary and BSE current. The BSE current was measured by applying a bias, V_T, of +50 V to the specimen, which retains any electron having a kinetic energy of less than 50 eV. The SE coefficient is defined as the ratio of the number of electrons exiting the specimen having a kinetic energy less than 50 eV to the number of primary electrons hitting the specimen. To measure this, the difference between the values of total yield with bias voltages of −50 V (ensuring that all secondaries along with BSEs were emitted from the specimen) and +50 V (ensuring that no secondaries escaped the specimen) was used (Reimer 1998). (Note that the value of 50 eV used for separating SEs from BSEs is somewhat arbitrary and historical, but is widely accepted in the literature and we used it for consistency). SE and BSE coefficients were then calculated from the Equations (2) and (3).

$$\text{BSE coefficient: } \eta = 1 + \frac{I_T(V_T = +50\text{ V})}{I_P} \quad (2)$$

$$\text{SE coefficient: } \delta_{0-50\text{ eV}} = \frac{I_T(V_T = -50\text{ V}) - I_T(V_T = +50\text{ V})}{I_P} \quad (3)$$

It is important to note that there are three main sources of SEs:

SE1—SE generated directly by primary electron in the specimen.

SE2—SE generated by BSE in the specimen.

SE3—SE generated by BSE hitting the SEM column or chamber wall.

Sometimes an outer collector electrode and a grid biased at −50 eV relative to the collector are used in order to prevent the SE3 contribution (Drescher *et al.* 1970; Reimer 1998). The accuracy of this method mainly depends on the backscattering coefficient of the collector and the transparency of the grid (Assa'd and EL-Gomati 1998; Reimer 1998; Reimer and Tolkamp 1980; Walker *et al.* 2008). Another method to minimize the SE3 contribution is to have a very small exposed area of the specimen (Reimer 1998; Reimer and Tolkamp 1980; Sim and White 2005). As the specimen surface (which is in our case $\sim < 8 \times 8\text{ mm}^2$) is much smaller than the collector surface (the entire SEM chamber wall in our setup), an SE3 generated at the SEM column or chamber wall by a BSE is very unlikely to hit the specimen again, but likely to be collected by the opposite side of the chamber wall and thus not contribute to the specimen current (Reimer 1998). Moreover, at negative specimen bias (−50 V or more negative), SE3 cannot make it back to the specimen and the only concern is for the positive bias value of +50 V (Sim and White 2005). However, as reported by Sim and White (Sim and White 2005), the contribution of such electrons toward TEY is very low (for gold—atomic number = 79—it is less than 3% and for silicon—atomic number = 14—about 1%). Given that BS yield decreases with the atomic number (Reimer 1998), we believe that SE3 is not significant for CNTs (less than 1%) and Equations (2) and (3) are valid in our experimental setup where exposure to SE3 was minimized. In addition, in the literature there is a very large variation in reported values of TEY, SE and BS coefficients. For example, for carbon, at 5 keV, TEY values in the range of 0.211–0.501—a variation of up to ~60%—have been reported (Joy 1995b). Also, even with the grid-collector method there could be an error due to the scattering from grid and collector (e.g. 0.3% error was estimated for a sample with no more than 3 mm in diameter (Assa'd and EL-Gomati 1998; Reimer and Tolkamp 1980). Given the above, we believe that the use of this experimental configuration (without grid and outer collector electrode) is justified. Furthermore, a similar experimental configuration was used for measuring SE and BSE coefficients by other authors (Huang *et al.* 2006; Sim and White 2005).

To characterize the experimental errors arising from the current measurements, we performed a series of assessments on the measurement setup. The nominal noise margin of the electrometer (Keithley 6517A) is 0.75 $fA_{p\text{-}p}$ (peak-to-peak). However, we observed a fluctuation of up to ~9 $fA_{p\text{-}p}$ over a period of 30 min (which is longer than the duration of any of our measurements) in the steady state when the electrometer was connected to the experimental setup with the primary beam of the SEM being off. The same measurement was also done with the primary beam on and no additional effect was seen on the noise level. The built-in filters (averaging and median filters) of the electrometer were enabled throughout the experiments to minimize the low current measurement errors. The averaging filter computes moving averages over ten data points taken at 16.67 ms intervals. The median filter takes the median of each set of three data points obtained from the averaging filter. To further increase the accuracy of the current measurements, each data point (for both primary and specimen

current) in our experiment was calculated from the average of ~100 of those filtered measurements, each taken at 1 s intervals. The primary beam and specimen currents were in the pico-ampere range (0.2–3 pA), which is much higher than the inherent noise level (<9 fA) of the setup. The primary current was measured both before and after the experiments at each primary energy to observe the effect of beam current fluctuations. For most of the primary energy range (1.5–20 keV), the beam currents were in the range of 1–3 pA and a variation of less than 4% was measured over the course of each experiment. For primary energies less than 1.5 keV, the beam currents were in the range of 0.2–1 pA and a variation of less than 10% was measured. The above errors and fluctuations were used to obtain the corresponding errors in our calculated TEY, BSE and SE coefficients, which appear as error bars on Figures 3, 4, 6 and 7. (For most data points the error bars are smaller than the curve markers and are masked by them).

Results and Discussion

Figures 3 and 4 show the TEY and SE coefficient, respectively, from a CNT forest having a diameter of 500 μm and length of ~1 mm for different biases and primary beam energies. The dotted vertical line indicates that the experiments in the 5–20 keV range were done in a separate sitting compared with the 0.4–5 keV experiments. The reason is that we had to change the SEM's anode after low-keV experiments to enable high-keV experiments. Therefore we had to vent the chamber in-between the two experiments. We kept all the conditions (sample location, working distance, etc.) exactly the same in both experiments to prevent potential variations. To ensure that the conditions were the same in both cases, we measured the data points for 5 keV during both experiments and observed a difference of less than 3%. Nonetheless, we added this dotted vertical line in the interest of providing the full experimental details. The dotted curve in Figure 3 (obtained with a bias of +50 V) represents the backscattering coefficient for the 500 μm-diameter forest. On the other hand, negative voltage applied to the sample favors the escape of SEs. As can be seen on the figure, as the negative bias is increased, more SEs acquire enough energy to overcome the vacuum barrier and a higher electron yield is obtained at each primary beam energy.

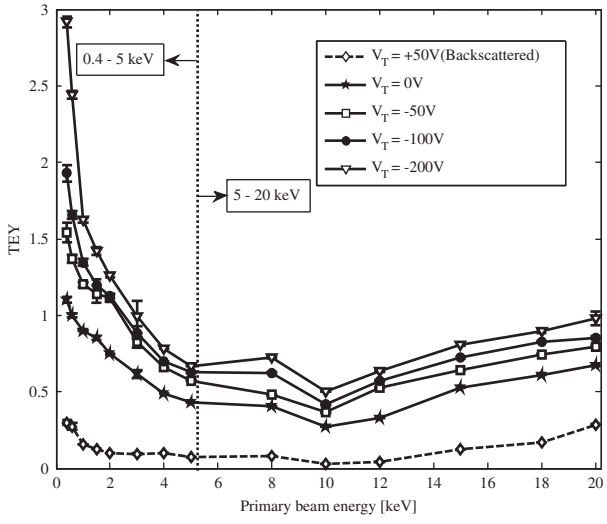

Fig 3. TEY from a carbon nanotube forest with a diameter of 500 μm. Legends show the corresponding applied voltages to the specimen. The dotted curve (diamond marker) represents the backscattering coefficient. The vertical line indicates that we had to exchange the anode in-between the low-keV and high-keV experiments. The 5 keV data points were measured in both experiments. They were very close (difference of less than 3%) and here the values obtained with the low-keV anode are plotted for the 5-keV point.

Figure 4 was obtained from Equation (3), namely by calculating the difference between the two curves with square (TEY at −50 V) and diamond (TEY at +50 V) markers in Figure 3. It is known that energy loss inside a bulk material decreases with increasing the primary beam energy (Goldstein *et al.* 1992; Reimer 1998). Hence, the total yield and SE coefficient should decrease with increasing beam energy after the maximum yield point, which is usually in the range of 0.1~1 keV for solid materials (Goldstein *et al.* 1992; Reimer 1998; Walker *et al.* 2008). A 500 μm-diameter solid cylinder should behave like a bulk for the energy range under consideration as the penetration range (in depth but also laterally) of electrons at such energies is only a few micrometers

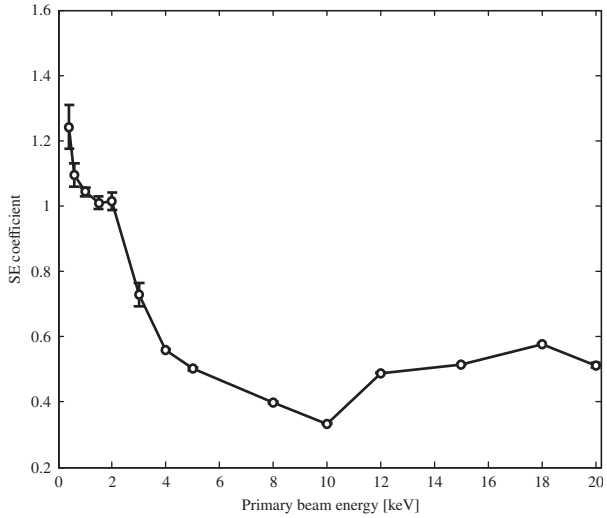

Fig 4. SE coefficient of the carbon nanotube forest with a diameter of 500 μm (obtained from Fig. 3 by calculating the difference between the curves of TEY at −50 V and +50 V).

in solids (e.g. ~5 μm for graphite at 20 keV (Goldstein *et al.* 1992; Kanaya and Okayama 1972; Sim and White 2005). Indeed, even for the nanotube forest the SE coefficient eventually decreases with primary energy after 18 keV (although we have only one data point beyond 18 keV for this specimen, the decrease in SE coefficient is quite obvious at 20 keV. In addition, the experimental results for the 50 μm-diameter forest, given later in this section, confirm that the SE coefficient eventually shows a decreasing trend with primary energy). However, the CNT forest exhibits a peculiar behavior in the intermediate range of primary energies: as can be seen from Figures 3 and 4, both the BSE and SE coefficients increase after 10 keV, in contrast with solid materials (the BSE coefficient in solids also decreases with the increase of primary beam energy for materials with low atomic number such as carbon (Joy 1995a; Reimer 1998)). We believe this happens because both high-energy electrons (BSEs) and low-energy electrons (SEs) can escape from the sidewalls in addition to the surface of the nanotube forest. This unusual behavior was not observed in the SE coefficient of a CNT carpet, where the lateral dimensions are so large that electrons in this primary energy range cannot escape from the sidewalls, measured by Huang *et al.* (Huang *et al.* 2006). However, given the 500 μm diameter of the forest used in our experiments, for this hypothesis to be true still a very high penetration range for primary electrons in the CNT forest is necessary. We believe this to be the case because of the porosity of the structure made up of many individual MWNTs. To estimate the inter-nanotube spacing, we performed an experiment of liquid-induced shrinkage of MWNT forests and the forests were found to shrink approximately 4.5 times after the liquid was introduced. Assuming that all the nanotubes in the forest have a diameter on the order of 10 nm (see Fig. 1(c)) and that the nanotubes were fully packed (hexagonal packing) after shrinking, we estimate an average distance of ~36 nm between two neighboring nanotubes in the original sample. A similar liquid-induced shrinkage was demonstrated by Futaba *et al.* for single-walled CNT forests (Futaba *et al.* 2006).

To investigate the hypothesis of unusually high electron range in the CNT forest, we performed Monte–Carlo simulations using the program NISTMONTE (Ritchie 2005). A 1.4 μm-diameter solid graphite cylinder was chosen to be simulated to compare with a cluster of 20 nm-diameter cylinders (representing nanotubes) having a gap of 40 nm between neighboring cylinders and an overall diameter of 1.4 μm (Fig. 5). The diameter of the "nanotubes" and the overall diameter were chosen according to computational limitations and do not correspond exactly to the experimental values.

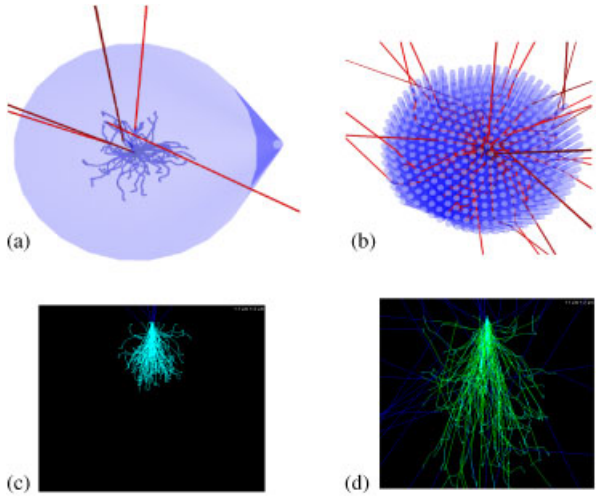

Fig 5. Monte-Carlo simulations showing the electron trajectories for comparison of electron range between a solid material and CNT forest at 5 keV. Among the 10,000 simulated trajectories, the first 50 are shown. (**a**) Top view of the trajectories in the solid graphite cylinder of 1.4 μm, (**b**) The same as (a) but for a cluster of nano graphite cylinders with a diameter of 20 nm each, having an overall cluster diameter of 1.4 μm, representing the CNT forest, (**c**) Side view of the trajectories in solid graphite and (**d**) Side view of the trajectories in the CNT forest.

However, as the simulations were performed at a primary beam energy of 5 keV at which the electron range is approximately 0.5 μm for graphite, they could still provide a qualitative insight into the variation of electron range between the two simulated structures.

10,000 electron trajectories were simulated for each structure at a 5 keV primary beam energy and it was found that the total BSE coefficient (including surface backscattering and sidewall escape) increased from ~0.08 in solid graphite (no sidewall scattering as the range is smaller than the diameter of the cylinder) to ~0.4 in the cluster mimicking the CNT forest. In the case of the CNT forest, both surface backscattering (~45% of the total BSEs) and sidewall escape (~55% of the total BSEs) happened, in agreement with our explanation for the increase in TEY, BSE and SE coefficients. In addition, it was also seen that surface backscattering was increased by ~10% because of the porous nature of the structure. For further investigation, the simulations were repeated at 6 keV primary beam energy (note that the range of primary electrons is still less than 1.4 μm in solid graphite at this energy). It was found that the total BSE coefficient was decreased to 0.077 in solid graphite, whereas it was increased to 0.65 in the cluster (surface backscattering decreased to ~38.5%, but sidewall escape increased to ~61.5%), again consistent with our explanation of the observed trend in BSE and SE coefficients based on the porosity of the forest.

The experiment was repeated with a nanotube forest of 50 μm in diameter for further validation of this hypothesis. The results are presented in Figures 6 and 7. It is seen that the minima of the TEY are shifted down to approximately 1.5 keV (for the 500 μm-diameter forest they were at about 10 keV). This shift seems to be primarily due to a similar shift in the SE coefficient (Fig. 7). This behavior is consistent with the previously discussed conjecture that the increase in the SE coefficient beyond a certain energy is due to the escape of secondaries from the sidewalls of the porous forest structure: for a forest with smaller diameter, it is expected that primary electrons with less energy will be able to reach the sidewalls of the forest to generate secondaries (for solid graphite the range is less than 0.1 μm at 1.5 keV). Also, eventually the SE coefficient starts decreasing with primary energy, like in bulk materials and in the case of the wider forest. However, this decreasing trend begins at a smaller primary energy (5 keV) compared with the wider forest (where the decreasing trend started at 18 keV).

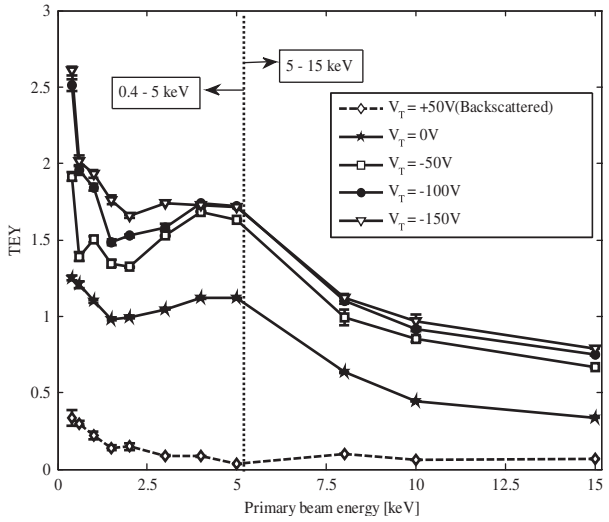

Fig 6. TEY from a carbon nanotube forest with a diameter of 50 μm. Legends show the corresponding applied voltages to the specimen. The dotted curve (diamond marker) represents the backscattering coefficient. The 5 keV data points were measured in both low-keV and high-keV experiments. They were very close (within 0.2%) and here the values obtained with the low-keV anode are plotted for the 5 keV point.

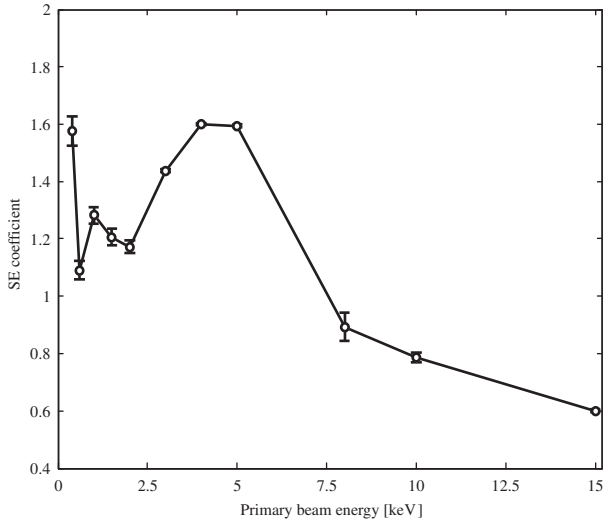

Fig 7. SE coefficient of the carbon nanotube forest with a diameter of 50 μm (obtained from Fig. 6—the difference between the curves of TEY at −50 V and +50 V).

Interestingly, and contrary to the case of the wider forest, the BSE coefficient does not increase with primary energy and stays almost constant slightly after the minimum point. We believe the reason behind this is that the length of the narrower forest is also much less than that of the wider one (about 100 μm as opposed to 1 mm: The shorter length in this case is due to the fact that the small-diameter forest cannot stand straight if made too long). Therefore, we expect that a large number of electrons easily reach the substrate and are captured by it, as opposed to escaping from the sidewalls of the forest and contributing to the emitted current. This also helps further explain the decrease in the SE coefficient after 5 keV: it appears that the BSE coefficient stays almost constant with increase in primary energy, implying that a constant number of primary or BSEs reach the sidewalls. However, as the energy of these electrons is increased, their energy loss to the sample is reduced, leading to a decrease in SE emission, like in bulk materials. As a final note, obviously with an almost constant BSE coefficient and decreasing SE coefficient with primary energy beyond 5 keV, the TEY also decreases, as seen on Figure 6.

It is worth mentioning that in addition to the qualitative deviation from secondary emission behavior in bulk materials discussed above, in general, electron yield from these forests was found to be higher than carbon, graphite and diamond-like-carbon films (Joy 1995b; Yamamoto *et al.* 2007; Walker *et al.* 2008). Table I shows a comparison between the SE yield from the nanotube forests and those other forms of carbon, as well as a few other materials.

As can be seen from Table I, nanotube forests do not have the highest pure SE emission yield (SE coefficient) of all the materials. However, they may have other advantages due to their structural strength and chemical stability. Moreover, as the total yield can be increased significantly by the application of bias (see Figs. 3 and 6), such nanotube structures can be considered as candidates for electron multipliers and vacuum transistors. Previously, we have observed highly enhanced secondary emission (electron yield greater than 100) from the tip of an individual nanotube lying on a

TABLE I A comparison of secondary electron emission coefficient between nanotube forests and other forms of carbon and several other materials

	Nanotube forest								
E (keV)	500 μm	50 μm	C	Graphite	DLC film	SiO_2	Au	MgO	GaAs
0.5	1.15	1.3	0.155	1.13	1.10	1.35	1.55	4.15	3.16
1.0	1.04	1.28	0.99	0.81	0.70	1.18	1.12	3.15	2.48
2.0	1.01	1.17	0.36	0.57	0.42	0.85	0.709	2.04	1.88
3.0	0.85	1.44	0.40	0.40	0.40	0.765	0.59	1.60	1.53
5.0	0.56	1.59	0.315	0.20	0.30	0.58	0.437	1.17	1.26

All the data have been taken from Joy's database (Joy 1995b) and references therein except for the DLC film (Yamamoto *et al.* 2007) and the nanotube forest (this study).

dielectric surface and biased near the threshold of field-emission (Nojeh *et al.* 2004). One of our long-term goals is to create structures using collections of nanotubes to obtain even higher electron gains as a potential candidate for vacuum nano-electronics. The present work focuses on the characterization of the TEY, SE and BSE coefficients as a preliminary step in that direction. If the observed behavior in our experiments is indeed because of the porosity of the structure as we suggested, then by controlling the nanotube density in the forest, one may be able to control the electron yield at different energies, which could have applications in energy-selective electron detectors and multipliers. In other words, the internal structure of the forest may provide an additional degree of freedom compared with bulk materials in designing electron emission devices. In addition, electron microscopy of nanoscale materials in itself can be an interesting and challenging problem, as charging and contamination could play a major, even dominant, role (Brintlinger *et al.* 2002; Finnie *et al.* 2008; Homma *et al.* 2004; Wong *et al.* 2006). A study of electron yield from nanostructures such as presented here can provide additional insight into imaging mechanisms and optimal imaging conditions (for example, the choice of the primary beam energy to reduce or prevent sample charging). Similar experiments on nanotube forests with different densities and other nanostructures like nanowire forests will be part of future work.

Conclusion

A systematic experimental study of electron yield from CNT forests was presented. Total yield, backscattered and secondary coefficients were measured from patterned CNT forests and an unusual behavior compared with bulk materials was observed. This is believed to be because of the unusually high range of electrons in nanotube forests, which could be ascribed to the porous nature of the nanotube forests. These results may present a useful step in the study of the interaction between electrons and nanotube collections for the development of various vacuum nano-electronic devices such as electron multipliers.

Acknowledgements

M. K. A acknowledges partial support from a University of British Columbia Graduate Fellowship.

References

Assa'd AMD, El-Gomati MM: Backscattering coefficients for low energy electrons. *Scanning Microscopy* **12**, 185–192 (1998).

Baroody EM: A theory of secondary electron emission from metals. *Phys Rev* **78**, 780–787 (1950).

Brintlinger T, Chen Y-F, Durkop T, Cobas E, Fuhrer MS, *et al.*: Rapid imaging of nanotubes on insulating substrates. *Appl Phys Lett* **81**, 2454–2456 (2002).

De Jonge N, Bonard J-M: Carbon nanotube electron sources and applications. *Phil Trans R Soc Lond A* **362**, 2239–2266 (2004).

De Jonge N, Oostveen JT, Teo KBK, Milne WI: The optical performance of carbon nanotube electron sources. *Phys Rev Lett* **94**, 186807-1–186807-4 (2005).

Dekker AJ: Variation of secondary electron emission of single crystals with angle of incidence. *Phys Rev Lett* **4**, 55–57 (1960).

Drescher H, Reimer L, Seidel H: Backscattering and secondary electron emission of 10–100 keV electrons and correlation to scanning electron microscopy. *Z Angew Phys* **29**, 331–336 (1970).

Finnie P, Kaminska K, Homma Y, Austing DG, Lefebvre J: Charge contrast imaging of suspended nanotubes by scanning electron microscopy. *Nanotechnology* **19**, 335202-1–335202-6 (2008).

Futaba DN, Hata K, Yamada T, Hiraoka T, Hayamizu Y, *et al.*: Shape-engineerable and highly densely packed single-walled carbon nanotubes and their application as super-capacitor electrodes. *Nat mater* **5**, 987–994 (2006).

Goldstein JL, Newburry DE, Echlin P, Joy DC, Roming Jr AD, *et al.*: Scanning Electron Microscopy and X-Ray Microanalysis: A Text for Biologists, Material Scientists and Geologists, Plenum Press, New York (1992).

Homma Y, Suzuki S, Kobayashi Y, Nagase M, Takagi D: Mechanism of bright selective imaging of single-walled

carbon nanotubes on insulators by scanning electron microscopy. *Appl Phys Lett* **84**, 1750–1752 (2004).
Hu B, Li P, Cao J, Dai H, Fan S: Field emission properties of a potassium-doped multiwalled carbon nanotube tip. *Jpn J Appl Phys* **40**, 5121–5122 (2001).
Huang L, Lau SP, Yang HY, Yu SF: Local measurement of secondary electron emission from ZnO coated carbon nanotubes. *Nanotechnology* **17**, 1564–1567 (2006).
Joy DC: Monte Carlo Modeling for Electron Microscopy and Microanalysis, Oxford University Press, New York (1995a).
Joy DC: A Database on electron-solid interactions. *Scanning* **17**, 270–275 (1995b).
Kanaya K, Okayama S: Penetration and energy-loss theory of electrons in solid targets. *J Phys D Appl Phys* **5**, 43–58 (1972).
Kim WS, Yi W, Yu S, Heo J, Jeong T, *et al.*: Secondary electron emission from magnesium oxide on multiwalled carbon nanotubes. *Appl Phys Lett* **81**, 1098–1100 (2002).
Lee J, Park J, Sim K, Yi W: Double layer-coated carbon nanotubes: Field emission and secondary-electron emission properties under presence of intense electric field. *J Vac Sci Tech B* **27**, 626–630 (2009).
McKay KG: Secondary Electron Emission. *Recent Advances in Electronics*, Academic Press, New York (1948).
Nojeh A, Wong WK, Yieh E, Pease RFW, Dai H: Electron beam-stimulated field-emission from single-walled carbon nanotubes. *J Vac Sci Tech B* **22**, 3124–3127 (2004).
Pendyala S, McGowan JW, Orth PHR, Zitzewitz PW: Detection of low energy positrons using spiraled electron multipliers. *Rev Sci Instrum* **45**, 1347–1348 (1974).
Reimer L: Scanning Electron Microscopy: Physics of Image Formation and Microanalysis, Springer, Berlin (1998).
Reimer L, Tolkamp C: Measuring the backscattering coefficient and secondary electron yield inside a scanning electron microscope. *Scanning* **3**, 35–39 (1980).
Ritchie NWM: A new Monte Carlo application for complex sample geometries. *Surf Interface Anal* **37**, 1006–1011 (2005).
Schou J: Secondary electron emission from solids by electron and proton bombardment. *Scan Microsc* **2**, 607–632 (1988).
Shapira D, Lewis TA, Hulett Jr. LD, Ciao Z: Factors affecting the performance of detectors that use secondary electron emission from a thin foil to determine ion impact position. *Nucl Instr and Meth A* **449**, 396–407 (2000).
Sim KS, White JD: New technique for in-situ measurement of backscattered and secondary electron yields for the calculation of signal-to-noise ratio in an SEM. *J Microsc* **217**, 235–240 (2005).
Walker CGH, El-Gomati MM, Assa'd AMD, Zadrazil M: The secondary electron emission yield for 24 solid elements excited by primary electrons in the range 250–5000 eV: a theory/experiment comparison. *Scanning* **30**, 365–380 (2008).
Wong WK, Nojeh A, Pease RFW: Parameters and mechanisms governing image contrast in scanning electron microscopy of single-walled carbon nanotubes. *Scanning* **28**, 219–227 (2006).
Yaghoobi P, Nojeh A: Electron emission from carbon nanotubes. *Mod Phys Lett B* **21**, 1807–1830 (2007).
Yamamoto K, Shibata T, Ogiwara N, Kinsho M: Secondary electron emission yields from the J-PARC RCS vacuum components. *Vacuum* **81**, 788–792 (2007).
Yi W, Yu S, Lee W, Han IT, Jeong T, *et al.*: Secondary electron emission yields from MgO deposited on carbon nanotubes. *J Appl Phys* **89**, 4091–4095 (2001).